A Hybrid Fluid-Particle Model for the Description of Ion Heating in High Mach Number Shock Waves.

R. Chodura

IPP 1/151 Oktober 1974

MAX-PLANCK-INSTITUT FÜR PLASMAPHYSIK

GARCHING BEI MÜNCHEN

MAX-PLANCK-INSTITUT FÜR PLASMAPHYSIK

GARCHING BEI MÜNCHEN

A Hybrid Fluid-Particle Model for the Description of Ion Heating in High Mach Number Shock Waves.

R. Chodura

IPP 1/151 Oktober 1974

Die nachstehende Arbeit wurde im Rahmen des Vertrages zwischen dem Max-Planck-Institut für Plasmaphysik und der Europäischen Atomgemeinschaft über die Zusammenarbeit auf dem Gebiete der Plasmaphysik durchgeführt.

R. Chodura

A Hybrid Fluid-Particle Model for the Description of Ion Heating in High Mach Number Shock Waves.

July 74

Abstract

A hybrid model treating electrons as a dissipative fluid and ions as particles is used to investigate numerically the properties of high Mach number magnetoacoustic shock waves propagating perpendicular to a magnetic field. Increasing the Alfvén Mach number M_A electron pressure behind the shock becomes bounded for $M_A \geq 15$. Ion reflectivity α increases but stays rather small even for $M_A \to \infty$, $B_o \to 0$ (i. e. $\alpha = 30 - 40$ % for reasonable collision frequencies in the shock). Thermalization of the shock by multiple bouncing in a cylindrical tube is studied for the case where the ion gyro-radii are large compared to the tube radius. Strong damping is found leading to equilibration after about two bounce oscillations. Ion reflection during first implosion is found to be essentially for non-adiabatic ion heating in the succeeding thermalization period.

1. Introduction

As is well known, driving a strong shock wave through a plasma is a very effective way of heating it to thermonuclear temperatures. Usually, the shock wave is launched by raising the magnetic field at the plasma boundary fast relative to the transit time of the disturbance through the finite plasma. A compression wave front then moves into the plasma, thus more or less abruptly changing the plasma parameters, such as density, velocity, temperature and magnetic field, from the undisturbed upstream state to the compressed, heated and inward moving state in the so-called piston region. The magnetic piston field of the vacuum region may penetrate into the piston region by resistive diffusion. Thus, in the compression wave a dynamic shock region and a diffusive piston region may be distinguished.

In the shock front, electrons and ions are heated in different ways and on different time and length scales. Electrons are accelerated mainly parallel to the shock front and undergo Ohmic friction with the ions, as a result of either classical electron - ion collisions or some kind of turbulence. This friction determines a scale length of shock transition with strong Ohmic heating of the electrons.

The ions, on the other hand, are heated preferentially by another mechanism. Owing to their large inertia they have a tendency to move freely through the resistive electron shock but are prevented from doing so by the electrons, which flow through the shock front barrier much more slowly in accordance with the motion of magnetic field lines and some diffusion due to their finite resestivity. Thus, an electric space charge

field is built up in the front, slowing down the ions to the same perpendicular velocity as the electrons. In running up the potential hill the velocity distribution of the ions is not only shifted towards smaller velocities (relative to the moving front), but also deformed, the small velocity wing being relatively enhanced. If the potential in the front were stationary and not too large and the instreaming ions were Maxwellian, the zeroth and second moments of the ion distribution in the front, n_i and T_i, would be related as $T_i \propto n_i^2$, i.e. as in a gas with one degree of freedom which is adiabatically compressed.

If the shock strength, i.e. the ratio of driving field to bias field ahead of the shock, exceeds some limit (depending on the upstream ion β), the potential jump in the shock front reaches such a value that some of the ions impinging on the shock front cannot overcome the potential barrier and are reflected with twice the front velocity [1]. The electrons, on the other hand, moving through the shock with the field lines and by resistive diffusion rather than free flight do not suffer this disintegration into reflected and transmitted components but follow the motion of the ions as a smooth, quasineutral background. Reflected ions may hit the shock front again either by gyration in the upstream magnetic field or simply by the geometric convergence effect of the shock front towards a plane or axis of symmetry, the latter effect being predominant in most shock experiments in cylindrical theta pinches. Ions can overcome the potential barrier at the second impact with the front and are, in the first case, thermalized by an ion beam instability. In the second case, they are reflected by the piston again and thermalize after multiple bouncing. In any case, ion reflection represents a very efficient mechanism of ion heating in shock waves. It is, therefore, worthwhile to investigate the conditions and efficiency of reflection under different conditions. This is done in Section 3.

It is clear that the behaviour of the ions, though related to viscosity, cannot be described by simple fluid and transport equations. A kinetic description is therefore required for the ions. In describing the electrons use can be made of the smallness of the gyro--radii and mean free paths as compared to the thickness of the shock front. Thus, moment equations suffice to describe the electrons. This hybrid model for ions and electrons is described in the following section.

2. Model

The electron component is described as a fluid subjected to some kind of friction with the ions (either classical or anomolous) which is characterized by a collision frequency ν . Electron inertia is neglected as compared to friction.

The electron momentum equation

$$-e\,(\underline{E} + \underline{v}_e \times \underline{B}) + m_e \nu\,(\underline{v}_i - \underline{v}_e) - \frac{1}{n_e}\nabla p_e = 0 \qquad (1)$$

determines the electric field $\underline{E}$. Work done against the friction force is transformed to internal energy of the electrons, thus raising the electron pressure p_e. Electron heat conduction is also included.

Ions are treated as particles using the particle-in-cell method. In this method, the orbits of a number of particles simulating ions are followed in their self-consistent fields. Then in each space-cell the moments of the ion distribution can be calculated to give the ion density n_i and the mean ion velocity v_i. The motion of the ions is assumed to be collision-free, the mean friction force $- m_e \nu\,(\underline{v}_i - \underline{v}_e)$ exerted by the electrons is applied to them as macroscopic force only.

The motion of electrons and ions is coupled by the assumption of quasineutrality,

i.e. $$n_i \simeq n_e \simeq n \qquad (2)$$

(the deviation from this equality being determined by the divergence of $\underline{E}$ in (1)). The dielectric current is consistently neglected.

The assumption of fluid electrons and the constraint of quasineutrality restricts the degrees of freedom of our model, and, hence, dispersion properties of the model for some kinds of waves and instabilities may differ from a real plasma. Thus, for instance, electron and ion oscillations are suppressed by condition (2). For numerical applications of the model this has the advantage that plasma frequencies need not be resolved. Propagation of ion acoustic modes is represented properly for $k\lambda_D \ll 1$ only, and unstable growth by electron resonance is excluded. Thus, the problem of anomalous resistivity in shock waves by current induced turbulence may not be treated by the model. On the other hand, magneto-acoustic modes and ion beam instabilities due to reflected ions are described properly in the limit $k\lambda_D \ll 1$.

The plasma is assumed to be initially extended uniformly in half-space (or within a plane slab or a cylinder) with density n_o and electron and ion temperatures T_{eo} and T_{io} respectively. The magnetic field at the beginning, B_o, is also assumed to be homogeneous and parallel to the confining wall or cylinder axis. At a time $t = 0$ the external field is suddenly changed to a value B_2 parallel to its initial direction and thereafter kept constant.

The development of the disturbance in the plasma is followed in one space coordinate x or r (and two velocity components). Thus, for instance, instabilities with $k_y = 0$ are not included.

In order to reduce the number of parameters in our equations, we normalize quantities as follows:

Distance x or r by $d_o = c/\omega_{po}$, where ω_{po} is the electron plasma frequency at density n_o; time t by $t_o = \omega_{c2}^{-1}$, where ω_{c2} is the electron gyrofrequency at magnetic field B_2; electron fluid velocity v_e, ion mean velocity v_i and ion particle velocity w by $v_o = d/t_o$; magnetic field B by B_2, electron pressure p_e by $n_o m_e v_o^2 = B_2^2 / 4\pi$.

Our system of equations then reads as follows:

$$d\underline{w}_i / dt = \mu\left\{ (\underline{w}_i - \underline{v}_e) \times \underline{B} - \frac{1}{n} \nabla p_e \right\}$$

$$\partial \underline{B} / \partial t = \nabla \times \left\{ \underline{v}_e \times \underline{B} - \eta \underline{j} + \frac{1}{n} \nabla p_e \right\}$$

$$\underline{j} = \nabla \times \underline{B} \qquad (3)$$

$$\underline{v}_e = \underline{v}_i - \underline{j} / n$$

$$\partial p_e / \partial t + \underline{v}_e \cdot \nabla p_e = -\gamma_e p_e \nabla \cdot \underline{v}_e + (\gamma_e - 1)\eta j^2 + (\gamma_e - 1) \nabla (\varkappa \nabla (p_e / n))$$

with the coefficients of resistivity and electron heat conduction

$$\eta = \nu / n, \quad \varkappa = 2 p_e / \{ \nu_* (1 + B^2 / \nu_*^2) \}$$

(ν_* may be different from υ because, unlike in the case of η, also electron-electron collsions contribute to $\varkappa$) and $\mu = m_e / m_i$.

The plasma has normalized density 1 and temperatures T_{eo} and T_{io} at the beginning. The external field jumps from initial value B_o to 1. Thus, our model depends on six parameters: B_o, T_{eo}, T_{io}, μ, ν, ν_*. If we treat a plane slab of finite thickness 2 L or a cylinder of radius R, another parameter $\varepsilon = (L / d)^2$ and $(R / d)^2$ respectively comes in.

In the following, we assume the initial electron temperature to be very small, assume an electron collision frequency $\nu_* = (1 + \frac{\sqrt{2}}{2}) \nu$ (as in case of Coulomb collisions), $\gamma_e = 5/3$ and adopt electron-proton mass ratio for μ. Thus, our model depends essentially

on the parameters B_o, ν, T_{io} and possibly ϵ.

3. Results

As was already pointed out, formation of a supercritical shock takes place in two time scales:

a) formation of a resistive shock due to dissipation in the electron fluid and reflection of some ions,

b) thermalization of the reflected ions.

Let us start with a description of phase a).

a) Ion reflection from a resistive shock.

After the driving field B_2 is applied, the external magnetic field diffuses into the resting plasma and starts to accelerate the field penetrated sheath. For not too large shock strength B_2 / B_o the density disturbance moves faster than the magnetic piston can follow and the shock separates into two parts, a shock front where the density, velocity, pressure and magnetic field change rather abruptly and a piston region where the magnetic field changes from the compressed state behind the front to the external value. After some time the shock front becomes stationary owing to a balance of field diffusion and the steepening effect of the dynamic term $\underline{v}_e \times \underline{B}$ in Ohm's law. The piston field stays diffusive and time-dependent.

Electrons are accelerated perpenciculary to the shock front by their Lorentz force and thermal pressure gradient. They transfer their perpendicular motion to the ions via a space sharge potential ϕ.

The spatial distributions of the magnetic field B and potential ϕ are shown in Fig. 1 for a shock with $B_2 / B_o = 7.1$ and an Alfvén Mach number $M_{Ao} = u_o / c_{Ao} = 5.7$, where u_o is the velocity of the shock front and c_{Ao} the upstream Alfvén speed. The shock structure in B with separated shock and piston regions is clearly developed. The front velocity $u_o / d_o \omega_{c2} = 1.88.10^{-2}$ is only slightly smaller (owing to ion reflection) than the value given by Rankine-Hugoniot conditions $\frac{1}{2}\sqrt{(\gamma_e + 1)\mu} = 1.91.10^{-2}$. The scale length of the front is given by

$$d \approx d_o^2 \nu / u_o \approx 2 (\nu / \omega_{c2}) d_o / \sqrt{(1+\gamma_e)\mu} \qquad (4)$$

Fig. 1 also shows the situation of the ions in an (x, w) - phase space, where w is the ion velocity in x direction. The front moves from left to right with velocity u_o. Ions encountered by the shock front are split into two components: one part is transmitted through the front and accelerated (in the mean) to the piston velocity $u_p = u_o - u_1$, where $- u_1$ is the flow velocity downstream from the shock in the shock frame. In crossing the shock ions are heated nearly adiabatically with $\gamma_i = 3$; behind the shock they transfer their thermal energy into the second degree of freedom by gyration, and so their x-temperature decreases behind the shock. The other component of the ions is reflected from the front with twice the front velocity $2 u_o$, approximately retaining its initial temperature T_{io}. The gyroradius of the reflected ions in the shock frame $r_g = u_o / (\mu \omega_{co})$ is fairly large compared to the shock thickness d

$$r_g / d = \frac{u_o^2}{\mu \omega_{co} d_o^2 \nu} \approx \frac{1}{4} (\gamma_e + 1) \frac{\omega_{co}}{\nu} \left(\frac{B_2}{B_o}\right)^2 \qquad (5)$$

As may be seen, in spite of the fairly high Mach number the fraction of reflected ions is rather small, i.e. 3 % in the case of Fig. 1.

What happens if the shock strength B_2 / B_o is still further increased, particularly in the limit $B_o \rightarrow 0$? This is shown in Fig. 2 for $B_2 / B_o = 20$ at 1.5 x the time and for the same ratio ν / ω_{c2} as in Fig. 1. As can be seen, the profiles of B and ϕ have changed qualitatively. The magnetic field of the shock front and piston region is no longer separated by a horizontal plateau, but the piston field now reaches the shock region with a finite slope B'. The discontinuity at the trailing edge of the shock front is conditioned by the copression of the upstream field B_o. This discontinuity therefore disappears completely for $B_o \rightarrow 0$, leaving a smooth monotonic profile for B. Though the upstream field B_o plays a decreasing role in the shock for increasing B_2 / B_o, the shock nevertheless does not become an acoustic one for $B_o \rightarrow 0$. The field diffusing from the piston region into the shock front rather takes over the role of the compressed bias field in lower Mach number shocks: it slows down the instreaming electrons relative to the shock and induces the current which is necessary in order to dissipate energy in the shock front. Ahead of the shock the well-known "foot" develops in the B profile. It is due to an electron flow required by the reflected ion beam in order to preserve quasineutrality. This electron flow carries some magnetic flux into the upstream region. For $B_o \rightarrow 0$ this foot disappears.

The profile of the electric potential ϕ shows another foot. This foot is caused by heat conduction rather than particle reflection: owing to the strong dependence of the perpendicular heat conductivity $\varkappa$ on the magnetic field (see equ. (3)) a reduction of the relative bias field B_o / B_2 keeping ν_* / ω_{c2} constant results in a strong increase of $\varkappa$ in the upstream region. Thus, an increasing portion of the electron thermal energy produced in the shock front can leak out into the upstream region, the slope of the temperature foot being given by

$$T_e' = n_o u_o (T_e / \varkappa) / (\gamma_e - 1) = \frac{1}{2} m_e u_o \nu_* (1 + \omega_{co}^2 / \nu_*^2) / (\gamma_e + 1) \qquad (6)$$

Since in the upstream region the potential is determined solely by the electron pressure, ϕ reflects the profile of p_e in this region.

One striking feature of the shock in Fig. 2 is the relatively strong ion reflection of about 24 % in the final steady state. As one can see from the particle density in different parts of the reflected beam, reflectivity was not constant in time, but small at the beginning, becoming larger as the shock proceeded. Owing to the enhancement of the ion reflection the front velocity and, hence, also the velocity of the reflected ions decreased.

Fig. 3 shows the dependence of some characteristic quantities behind the shock on the shock strength B_2 / B_o. The shock velocity u_o is given by the upstream Alfvén Mach number M_{Ao} and also by $M_{A2} = M_{Ao}\, B_o / B_2$, i.e. u_o divided by the Alfvén speed at the driving field B_2 and density n_o. For small shock stength, i.e. $B_2 / B_o \leqslant 5$, the quantities behave as given by simple Rankine-Hugoniot conditions: M_{A2} decreases towards a limit $M_{A2}^2 \rightarrow (\gamma_e + 1) / 4$ (indicated by a dashed line), while the potential ϕ increases very sharply, passes a maximum and also tends towards a limiting value from above. For higher shock strength this behaviour is changed owing to the onset of ion reflection. This effect slows down the front velocity M_{A2} and, as a consequence of decreased onstreaming energy $m_i\, u_o^2 / 2$, the front potential ϕ_1 as well as the electron pressure p_{e1} is prevented from rising indefinitely with increasing shock strength as required by simple Rankine-Hugoniot conditions, but tends toward a saturation value of about 0.84 of the energy density of the driving field. The compression ratio of the density and magnetic field, n_1 / n_o and B_1 / B_o respectively, exceeds the limiting value $(\gamma_e + 1) / (\gamma_e - 1) = 4$ of the Rankine-Hugoniot conditions. Because the shock profile of B does not separate from the piston by a horizontal plateau for large B_2 / B_o (Fig. 2), the condition $B_1 / B_o = n_1 / n_o$ does not hold any longer in this regime.

Ion reflection is measured by a coefficient α

$$\alpha = \frac{\dot{N}}{n_o u_o} \qquad (6)$$

where $\dot{N}$ is the number of reflected ions per area and time. This number is, even for high Mach numbers, surprisingly low, e.g. less than 10 % for $M_{Ao} < 8$. This has to be compared with results from a dissipationless, cold electron, cold ion hybrid model which exhibits total reflection of instreaming ions for Mach numbers $M_{Ao} > 3.18$ [2]. This so-called upper critical Mach number is even lowered for finite upstream ion temeratures [3]. The difference in our results is, of course, due to the additional possibility of dissipating onstreaming plasma energy into the electrons in the present model. According to the rather small degree of ion reflection, the front velocity M_{A2} stays well above the value from a so-called "free-particle model" (where all ions are assumed to be reflected), which would by $M_{A2} = 1/2$. Simulated ion reflectivities for $B_o = 0$ agree qualitatively well with those obtained in collisionless shock experiments, i.e. $\alpha \approx 35$ % [4] or even less [5].

From the equs. (3) describing the shock in normalizing units it follows that ion reflectivity α can only depend on ν, T_{io} and B_o. On the other hand, α is determined by ion-streaming energy and -temperature ahead of the shock in relation to the shock potential $[\phi]$, where $[\ ]$ means the difference of a quantity behind and ahead of the shock. From electron energy equation, assuming stationarity, one can derive

$$[\phi] - \frac{B_o}{4\pi n_o}[B] - \frac{\gamma_e}{\gamma_e - 1}\left[\frac{p_e}{n}\right] = 0 \qquad (7)$$

which expresses $[\phi]$ by the jump values of B, p_e, and n. From mass-, momentum-, energy- and flux conservation (including the reflected ion beam) one can get these quantities

without specifying the strength of dissipation, i. e. ν . Thus α is completely determined by quantities which are independent of ν hence for a stationary shock α is independent of ν .

As was shown in Fig. 2, for high shock strength $B_2 / B_o \geq 7$ piston and shock region link together and some flux diffuses from the piston into the shock region. This makes the shock slightly instationary and equ. (7) does not hold exactly anymore. Thus α becomes dependent on ν . Fig. 4 shows this dependence on ν together with the dependence on T_{io} for the case $B_o = 0$. In the limit of very small ν , i.e. for ν approaching the lower hybrid frequency, α must increase rather abruptly to the values found for dissipationless electrons in [2] and [3].

On the other hand, α is also very sensitive on the efficiency of electron heating in the shock front. If a fraction of Joule heating is lost (for instance due to axial heat conduction along the magnetic field) ion reflectivity is increased.

b) Thermalization of reflected ions.

As was noted in the preceding part ions transmitted into the piston region are heated only adiabatically. Thus only the energy fed into the reflected ion beam may act as a source for non-adiabatic ion heating when the beam is thermalized.

This can happen when the reflected ions after a gyration in the upstream magnetic field re-enter the shock front and are transmitted into the piston region where they are slowly thermalized by an ion-beam instability [6, 7, 8].

In many laboratory (pinch-) experiments the shock forms an imploding cylinder, thus reflected ions are enforced geometrically to re-enter the shock front even when ion gyro-radii are large as compared to the diameter of the cylinder. (A necessary condition for shock formation and creation of reflected ions in this cylindrical case is that the shock thickness d should fit into the tube radius R , i.e. that magnetic Reynolds number is large).

Fig. 5 shows some snapshots of ion motion in phase space together with magnetic field and potential for implosion and thermalization in a cylindrical shock with $B_o = 0$. Reflected ions, moving on nearly straight lines (Fig. 5b) approach the axis are reflected and hit the shock front again (Fig. 5c) with an increased relative velocity ($\sim 3\, u_o$) and thus can penetrate the shock. The shock is turned back at the axis and reflected ions penetrate into the plasma-free piston area and are reflected there again (Fig. 5d). They thus form a cloud of fast ions around the shocked, dense plasma. The latter expands after maximum compression (Fig. 5e) and is compressed again, forming a weaker shock with some ion reflection at second compression (Fig. 5f). After the second compression the whole plasma is nearly thermalized, the electric potential now being nearly uniform (Fig. 5i).

In Fig. 6 different kinds of energies per particles, averaged over velocity and space, are plotted as functions of time. The second moment of the ions, W^i_{th} comes up when ions are reflected from the shock front, it increases again when ions are reflected from the axis. It ends up at about 2.4 % of the total energy (including field energy W_f within the tube).

Fig. 7 shows the radial distribution of magnetic field, density, temperatures and azimuthal velocity of the plasma at a final state. As may be seen, the plasma is moderately compressed. The magnetic field is excluded from the inner region, $\beta = 8\pi(p_i + p_e)/B_2^2 \approx 1$ at the axis. Electron temperature is about 8 times higher than ion temperature and uniformly distributed. This latter result is not supported by findings in theta pinch shock experiments [9], where electron temperature is found to be comparably to ion temperature and restricted to the current sheath. The difference may be due to the modification of collision frequency under changing plasma conditions, to axial electron heat losses and a reduced radial heat conduction presumeably due to residual magnetic field from preionization. As the radial electric field has disappeared, ions are free to gyrate in the magnetic field giving rise to opposite rotation of the inner and outer parts of the plasma.

Of course the detailed structure of the radial distribution of plasma quantities will depend on the functional dependence of ν on plasma parameters. So Fig. 7 only gives a qualitative picture.

4. Conclusion

Non-adiabatic ion heating in pinches is conditioned by efficient ion reflection from the magnetoacoustic shock front during compression. The preceding results using a hybrid model of Vlasov ions and a dissipative electron fluid show rather imperfect ion reflection from the shock front. As a consequence a large fraction of onstreaming plasma energy is fed into internal energy of the electrons. This is in contrast to earlier results

using a hybrid model without electron dissipation showing total ion reflection at rather small Mach numbers. Thus it appears quite important to include the processes connected with the electrons, i.e. electron-ion friction, Joule heating and heat losses in order to get results comparable to shock and pinch experiments. The validity of estimates on ion heating in pinches based on a "free-particle (perfect ion reflection) model" seem rather doubtful.

Acknowledgement

The author wishes to thank B. Röthlein and Dr. W. Schneider for their help in preparing the program.

Fig. 1) Magnetic field B (x), electric potential ϕ (x) and ion position in a (x, w) -phase plane for a plane shock wave with $B_2 / B_o = 7.1$, $M_{Ao} = 5.8$, $\nu / \omega_{c2} = 0.025$, $T_{io} / (B_2^2 / 4\pi n_o) = 5.10^{-5}$.

Fig. 2) The same as Fig. 1 but $B_2 / B_o = 15$, $M_{Ao} = 10.4$

Fig. 3) Quantities behind the shock front together with Alfvén Mach numbers $M_{Ao} = u_o / (B_o^2 / 4\pi n_o m_i)^{1/2}$ and $M_{A2} = u_o / (B_2^2 / 4\pi n_o m_i)^{1/2}$ as function of the shock strength B_2 / B_o for $\nu / \omega_{c2} = 0.025$, $T_{io} / (B_2^2 / 4\pi n_o) = 5.10^{-5}$

Fig. 4) Ion reflectivity α at $B_o = 0$ for different values of ν / ω_{c2} and $T_{io} / (B_2^2 / 4\pi n_o)$

Fig. 5a - i) Ion distribution in phase space at different states of acceleration and thermalization together with B and ϕ ($B_o = o$, $\nu / \omega_{c2} = 0.05$, $T_{io} / (B_2^2 / 4\pi n_o) = 5.10^{-4}$, $(R / d_o)^2 = 5.10^3$)

Fig. 6) Time behaviour of space averaged mean energies per particle for Fig. 5: W_f = energy of magnetic field, W^i_{kin} = kinetic ion energy, W^i_{th}, W^e_{th} thermal ion and electron energy respectively.

Fig. 7) Radial distribution of different quantities at $t = 1.9.10^4\, \omega_{c2}^{-1}$ of Fig. 5

Literature

[1] SAGDEEV, R. Z., Review of Plasma Theory (M.A. LEONTOVICH ed.), vol.4, p. 23, New York, 1966

[2] FORSLUND, D.W., FREIDBERG, J.P., Phys. Rev. Letters, 27, 1189 (1971)

[3] MASON , R.J., Ph. Fluids 15 , 1082 and 2072 (1972)

[4] SÖLDNER, F., Report Nr. IPP 141, Garching (Germany), 1974

[5] HÖTHKER, K., DIETZ, K.J., DIPPEL, K.H., HINTZ, E., Proc. 6th Europ. Conf. on Controlled Fusion and Plasma Physics, Moscow 1973, p. 299

[6] AUER, P.L., HURWITZ, H., KILB, R.W., Phys. Fluids, 5 , 298 (1962)

[7] BISKAMP, D., WELTER, H., Nucl. Fusion 12 , 663 (1972)

[8] PAPADOPOULOS, K., WAGNER, C.E., HABER, I., Phys. Rev. Letters, 27 , 982 (1971)

[9] KEILHACKER, M., KORNHERR, M., NIEDERMEYER, H., SÖLDNER, F., STEUER, K.-H., Proc. 6th Europ. Conf. on Controlled Fusion and Plasma Physics, Moscow, 1973, p. 303

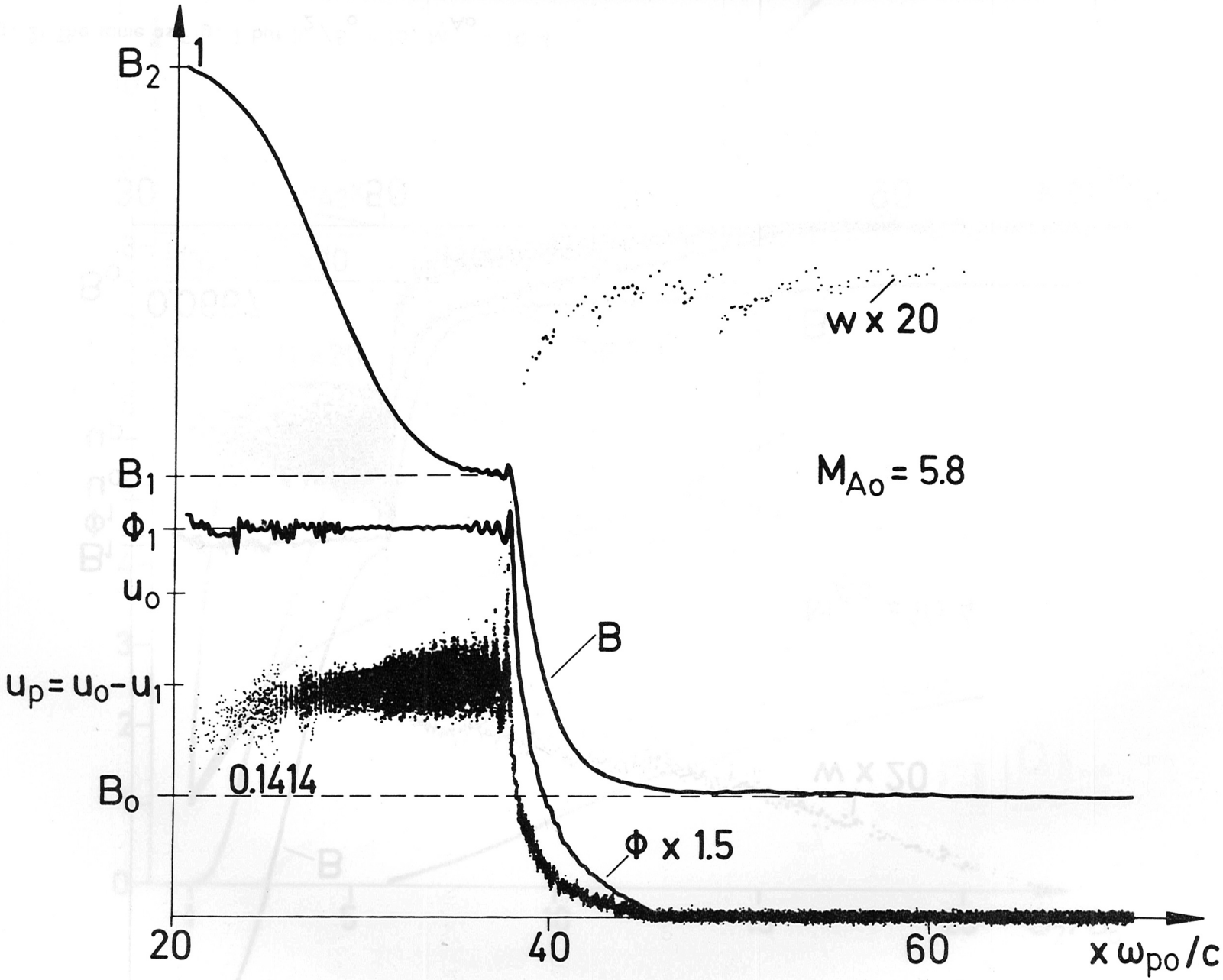

Fig. 1) Magnetic field B (x), electric potential ϕ (x) and ion position in a (x, w) -phase plane for a plane shock wave with $B_2 / B_o = 7.1$, $M_{Ao} = 5.8$, $\nu / \omega_{c2} = 0.025$, $T_{io} / (B_2^2 / 4\pi n_o) = 5.10^{-5}$.

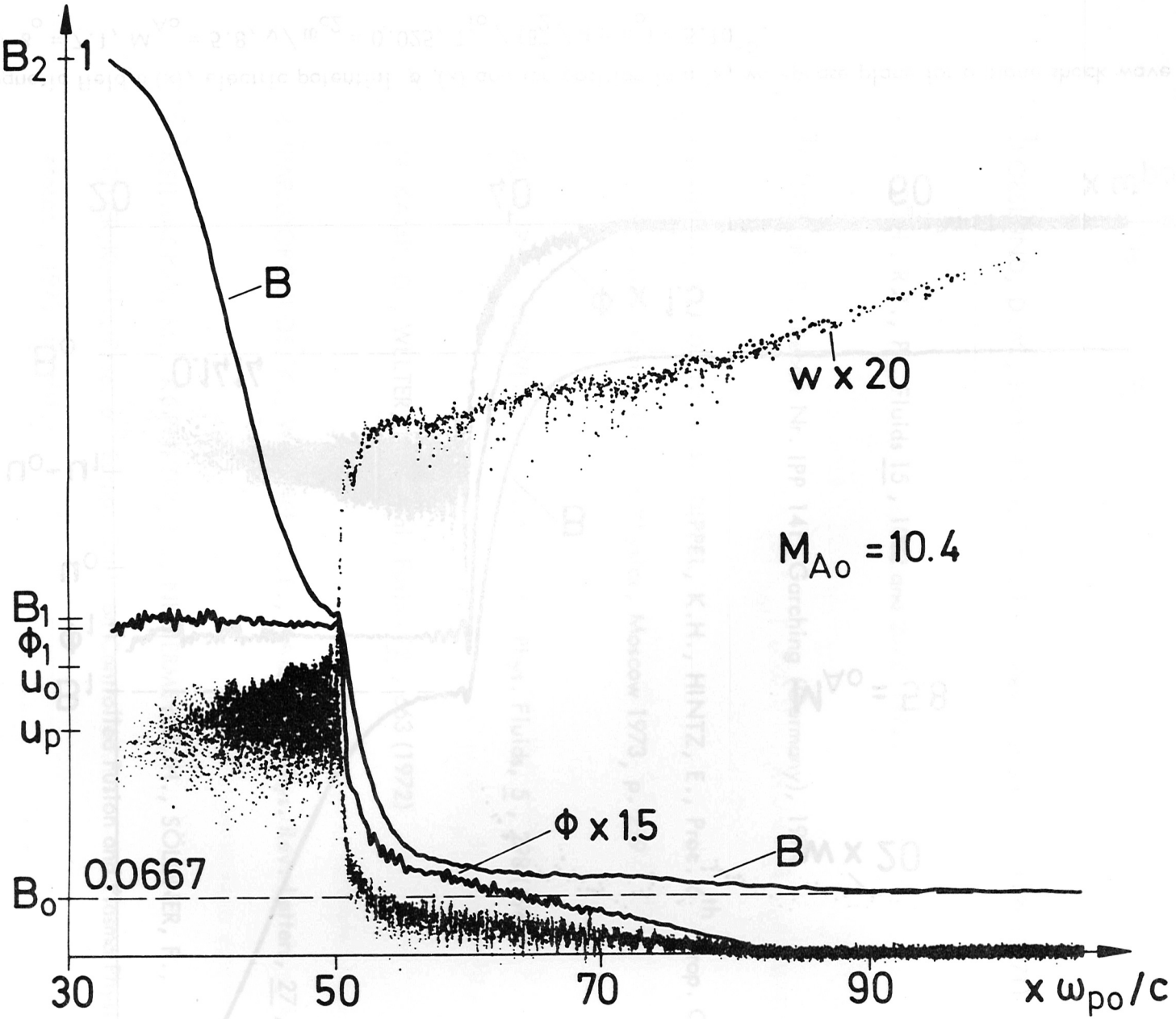

Fig. 2) The same as Fig. 1 but $B_2/B_o = 15$, $M_{Ao} = 10.4$

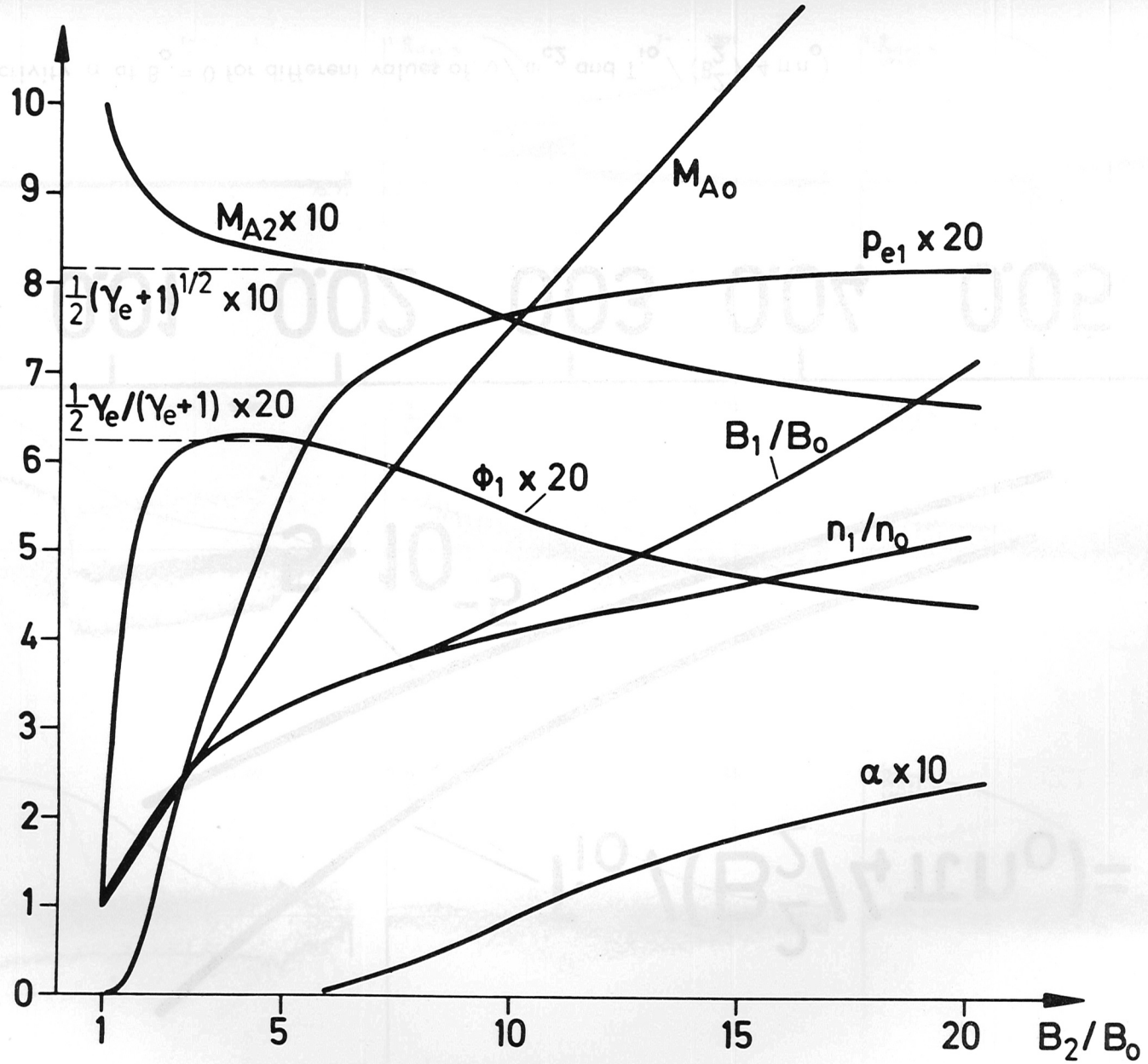

Fig. 3) Quantities behind the shock front together with Alfvén Mach numbers $M_{Ao} = u_o / (B_o^2 / 4\pi n_o m_i)^{1/2}$ and $M_{A2} = u_b/(B_2^2/4\pi n_o m_i)^{1/2}$ as function of the shock strength B_2 / B_o for $\nu / \omega_{c2} = 0.025$, $T_{io} / (B_2^2 / 4\pi n_o) = 5.10^{-5}$

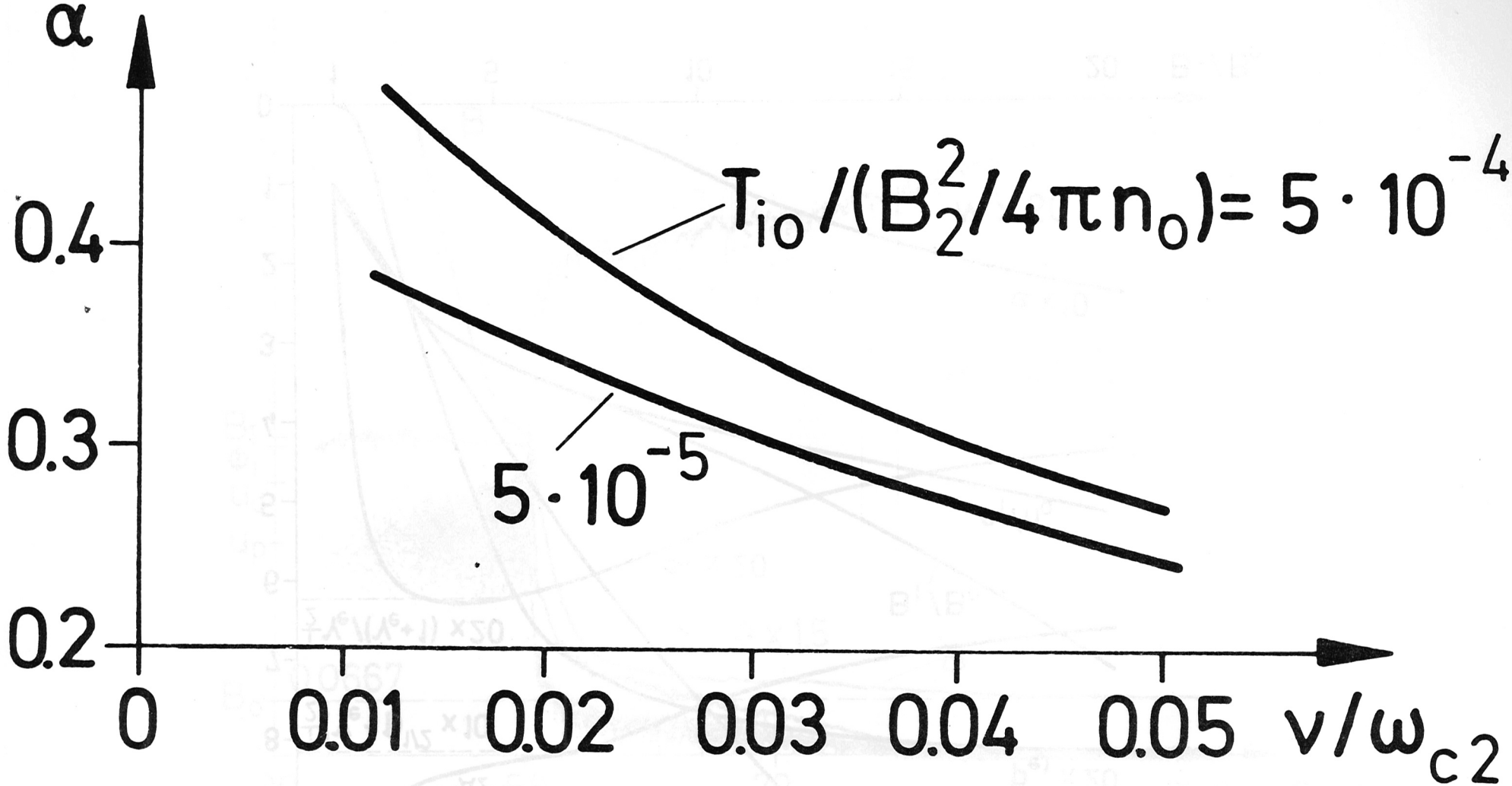

Fig. 4) Ion reflectivity α at $B_o = 0$ for different values of ν/ω_{c2} and $T_{io}/(B_2^2/4\pi n_o)$

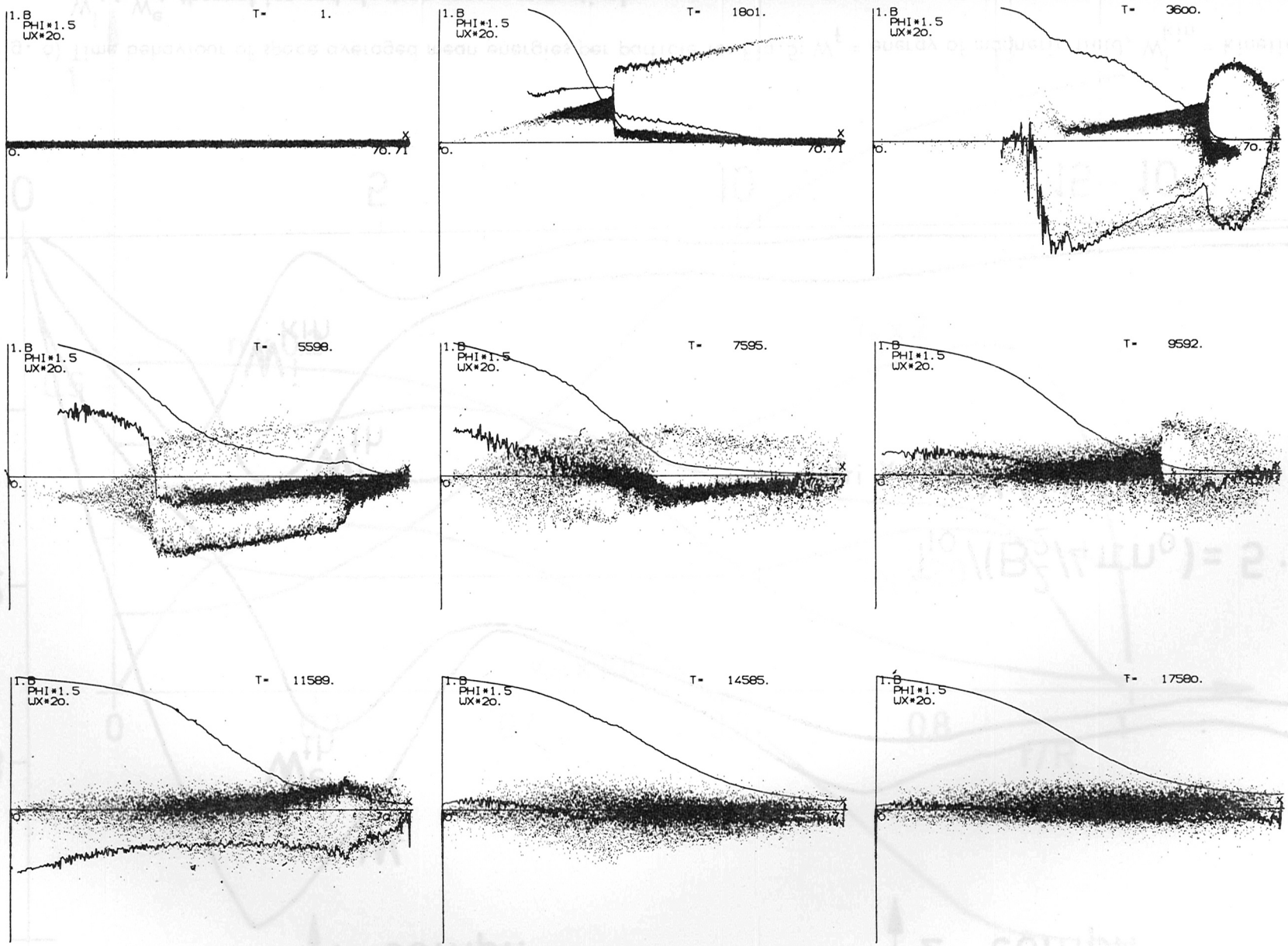

Fig. 5a-i) Ion distribution in phase space at different states of acceleration and thermalization together with B and ϕ

$(B_o = o,\ \nu / \omega_{c2} = 0.05,\ T_{io} / (B_2^2 / 4\pi n_o) = 5.10^{-4},\ (R / d_o)^2 = 5.10^3)$

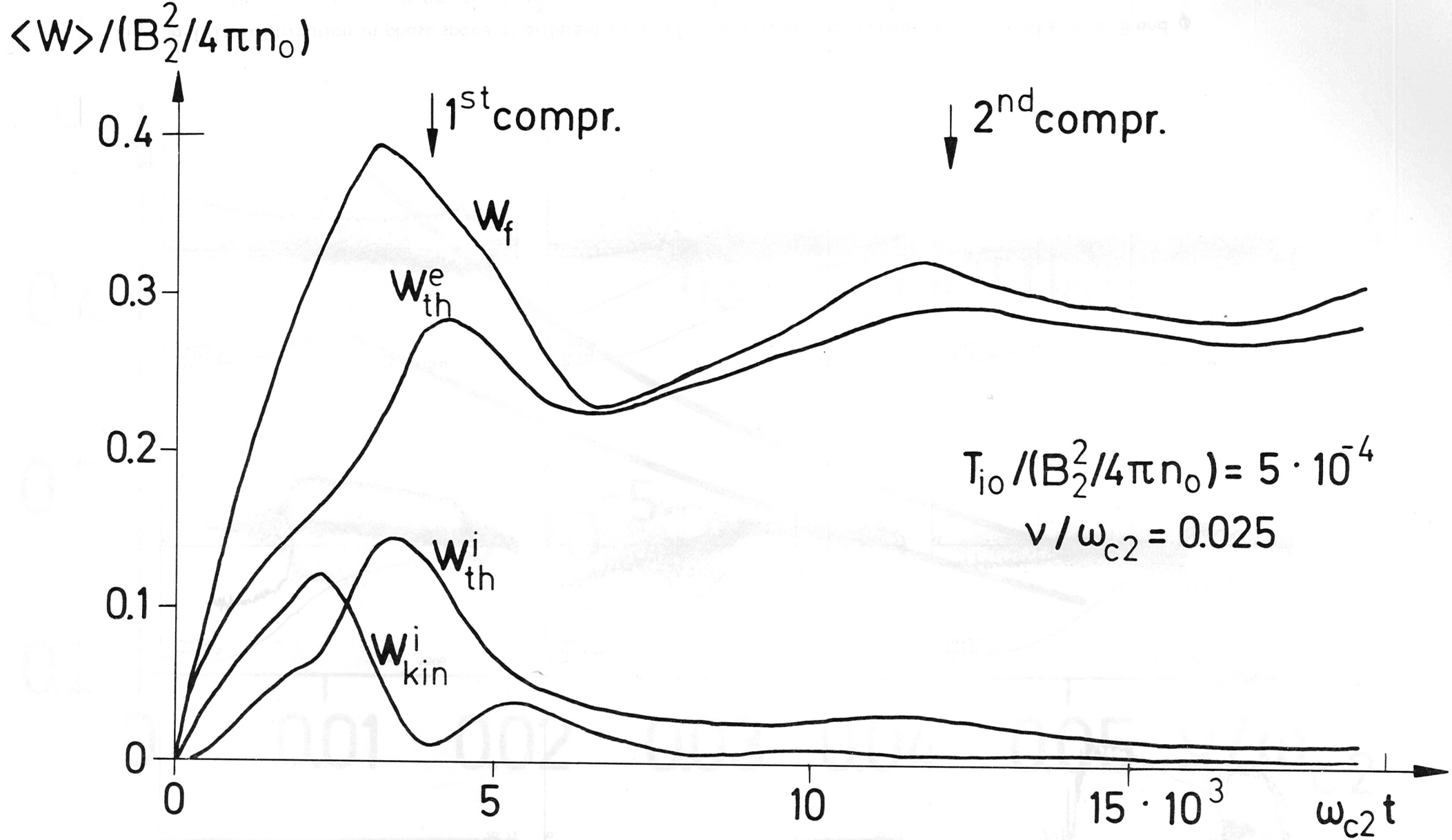

Fig. 6) Time behaviour of space averaged mean energies per particle for Fig.5: W_f = energy of magnetic field, W^i_{kin} = kinetic ion energy, W^i_{th}, W^e_{th} thermal ion and electron energy respectively

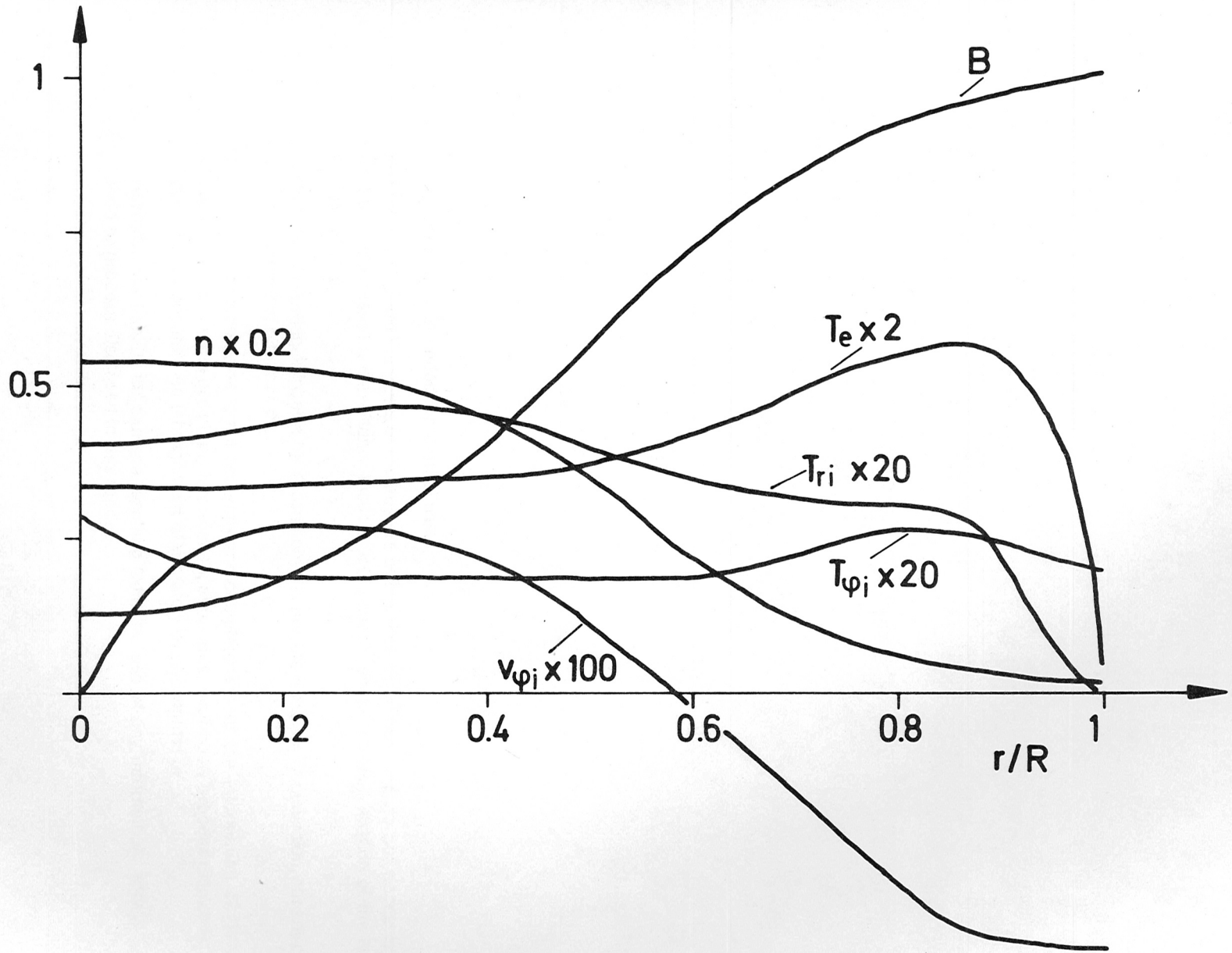

Fig. 7) Radial distribution of different quantities at $t = 1.9.10^4\ \omega_{c2}^{-1}$ of Fig. 5